ACS Chemical Neuroscience

Research Article

pubs.acs.org/chemneuro

# Multicolor Fluorescence Imaging of Traumatic Brain Injury in a Cryolesion Mouse Model

Bryan A. Smith,[†,∥] Bang-Wen Xie,[‡,∥] Ermond R. van Beek,[‡] Ivo Que,[‡] Vicky Blankevoort,[‡] Shuzhang Xiao,[†] Erin L. Cole,[†] Mathias Hoehn,[§] Eric L. Kaijzel,[‡] Clemens W. G. M. Löwik,*[,‡] and Bradley D. Smith*[,†]

[†]Department of Chemistry and Biochemistry, 236 Nieuwland Science Hall, University of Notre Dame, Notre Dame, Indiana 46556, United States

[‡]Molecular Endocrinology and Molecular Imaging, Department of Endocrinology, Leiden University Medical Center, Albinusdreef 2, 2333 ZA Leiden, The Netherlands

[§]Max Planck Institute for Neurological Research, Gleuelerstrasse 50, D-50931, Cologne, Germany

*Supporting Information*

**ABSTRACT:** Traumatic brain injury is characterized by initial tissue damage, which then can lead to secondary processes such as cell death and blood-brain-barrier disruption. Clinical and preclinical studies of traumatic brain injury typically employ anatomical imaging techniques and there is a need for new molecular imaging methods that provide complementary biochemical information. Here, we assess the ability of a targeted, near-infrared fluorescent probe, named PSS-794, to detect cell death in a brain cryolesion mouse model that replicates certain features of traumatic brain injury. In short, the model involves brief contact of a cold rod to the head of a living, anesthetized mouse. Using noninvasive whole-body fluorescence imaging, PSS-794 permitted visualization of the cryolesion in the living animal. Ex vivo imaging and histological analysis confirmed PSS-794 localization to site of brain cell death. The nontargeted, deep-red Tracer-653 was validated as a tracer dye for monitoring blood-brain-barrier disruption, and a binary mixture of PSS-794 and Tracer-653 was employed for multicolor imaging of cell death and blood-brain-barrier permeability in a single animal. The imaging data indicates that at 3 days after brain cryoinjury the amount of cell death had decreased significantly, but the integrity of the blood-brain-barrier was still impaired; at 7 days, the blood-brain-barrier was still three times more permeable than before cryoinjury.

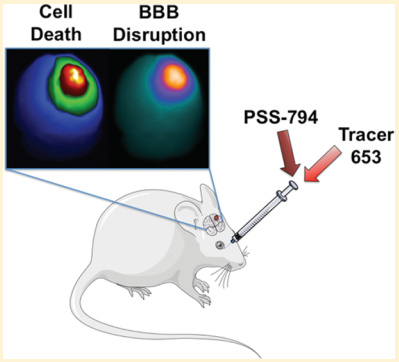


**KEYWORDS:** *Traumatic brain injury, multicolor fluorescence imaging, cell death imaging, blood-brain-barrier, annexin V, zinc(II)-dipicolylamine*

Traumatic brain injury (TBI) is a major public health concern in the United States with 1.7 million people sustaining a TBI annually.[1] Over 2% of the United States population is believed to experience TBI-associated disabilities, accounting for approximately $60 billion annually in direct and indirect costs.[2] TBI is a highly heterogeneous disorder that can manifest different pathophysiological changes depending on the type, severity, and location of the brain injury. TBI is typically characterized in two stages: (1) the primary injury at the site of impact which results in tissue damage and hemorrhaging, and (2) the delayed secondary insult that represents nonmechanical damage due to continuous pathological processes.[3] These pathological processes include blood-brain-barrier disruption, edema, oxidative stress, inflammation, and cell death.[3] Clinical presentation of the secondary insult is usually delayed and believed to be sensitive to therapeutic intervention. Thus, the secondary pathological processes may be viable options as therapeutic and imaging targets for treatment and diagnosis of TBI.

In the clinic, computer tomography and magnetic resonance imaging are routinely used for brain imaging of TBI.[4,5] Both modalities rely on morphological changes which occur later in the disease process; thus, TBI diagnosis and prognosis would be better served using molecular imaging techniques that target early stage biochemical changes.[6] Fluorescence optical imaging is an attractive option for preclinical research due to its inherent safety and high sensitivity, but very few optical imaging probes have been evaluated in animal models of TBI.[7] There is a specific need for deep-red and near-infrared fluorescent probes that allow relatively deep penetration of the light through skin and tissue. An attractive concept is the possibility of multicolor imaging using multiple probes in a single animal, each probe with its distinctive wavelength and ability to report on different biomolecular processes. At present, there is a small but growing number of literature examples of simultaneous multicolor in

**Received:** February 9, 2012
**Accepted:** April 7, 2012
**Published:** April 7, 2012

vivo optical imaging.[8−10] In the case of TBI, imaging studies would be greatly facilitated by the development of protocols that employ a mixture of a targeted probe for cell death and a nontargeted tracer for blood-brain-barrier (BBB) permeability. This requires two sets of technical advances: (1) development and validation of deep-red and near-infrared fluorescent imaging and tracer probes that enable multicolor in vivo imaging in living animals, and (2) straightforward preclinical TBI models that are amenable to optical imaging. Here we address both needs by adapting a preclinical mouse model for TBI and investigating a set of complementary fluorescent imaging probes.

Numerous fluorescent imaging probes have been developed to specifically target biomarkers associated with cell death, but the most popular biomarker for in vivo imaging is phosphatidylserine exposure on the plasma membrane.[11−13] Imaging results with protein-based probes are promising, but technical problems such as the poor pharmacokinetics have combined to limit translation into the clinic.[14−17] It is quite challenging to alter the pharmacokinetics of proteins, so there is motivation to develop cell death imaging probes with low molecular weight.[18−20] We have contributed to this research topic by designing synthetic fluorescent zinc(II)-dipicolylamine probes that can distinguish the anionic membranes of dead and dying cells over the near neutral membranes of healthy cells.[21] To facilitate in vivo imaging, we developed PSS-794, a zinc(II)-dipicolylamine probe containing a near-infrared carbocyanine fluorophore. PSS-794 can identify cell death in a number of animal models.[22−24] In this current study, we demonstrate the ability of PSS-794 to noninvasively detect cell death in a brain cryolesion TBI mouse model using whole-body, epifluorescence imaging. Specifically, we compare cell death imaging performance of PSS-794 and fluorescently labeled Annexin V, a well-known protein-based probe for cell death imaging.[25] We also describe the nontargeted, deep-red dye, Tracer-653, for monitoring blood-brain-barrier disruption, and a binary mixture of PSS-794 and Tracer-653 for multicolor imaging of cell death and blood-brain-barrier permeability in a single animal.

## RESULTS

The study examined four fluorescent imaging probes (Figure 1). Two of the probes, the synthetic zinc(II)-dipicolylamine complex, PSS-794, and the dye-labeled protein, Annexin-Vivo 750, are known to selectively target the anionic membranes of dead and dying cells via bridging cations (zinc and calcium, respectively). It is worth noting that PSS-794 is formulated as a zinc complex primarily to improve water solubility. Although the zinc complex is labile, the bloodstream concentration of $Zn^{2+}$ (10−20 $\mu$M) is high enough to not limit the three component assembly of apo-PSS-794, $Zn^{2+}$, and phosphatidylserine at the membrane surface.[26] The other two probes, Tracer-794 and Tracer-653, are nontargeted fluorophores that diffuse through the blood pool and, thus, serve to measure permeability of the BBB.[27,28] Tracer-794 has the same near-infrared fluorophore as PSS-794 and so is an excellent control compound to evaluate the effect of the attached zinc(II)-dipicolylamine targeting unit. Tracer-653 is a bright and stable deep-red dye that does not self-aggregate or associate with serum proteins. Furthermore, it has a narrow emission band that can be monitored simultaneously with near-infrared PSS-794 in the same animal using different imaging filter sets (filter sets for PSS-794: ex, 705−780 nm; em, 810−885 nm; filter sets for Tracer-653: ex, 615−665 nm; em, 695−770 nm). The

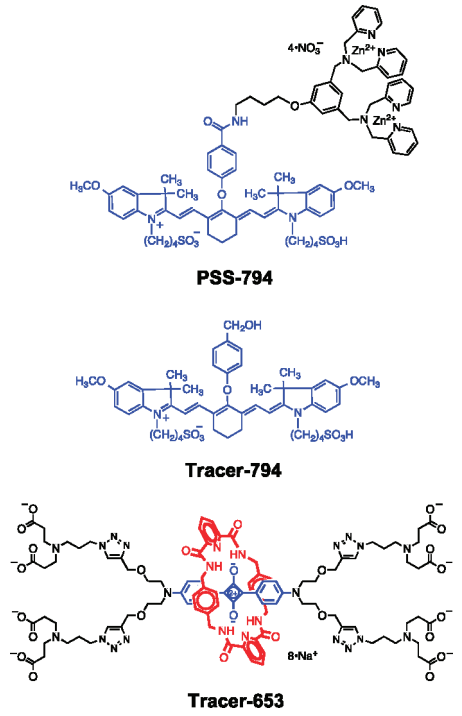


**Figure 1.** Chemical structures of PSS-794, Tracer-794, and Tracer-653.

specific targeting of the four fluorescent probes was tested in an adapted brain cryolesion mouse model that induces rapid breakdown of the BBB causing vasogenic brain edema and tissue damage.[29] In short, two separate cohorts of athymic mice (n = 5) were anesthetized by isoflurane inhalation. A metal cylinder with a 3 mm diameter was precooled in liquid nitrogen and applied to each mouse's head for 60 s. Individual mice then received an intracardiac injection of either PSS-794 (3.0 mg/kg), Tracer-794 (3.0 mg/kg), or Annexin-Vivo 750 and were imaged in an IVIS Spectrum instrument at 3 h, 6 and 24 h postprobe injection. Figure 2 shows representative images at the different time points. Immediately after probe injection, there is apparent accumulation of Tracer-794 at the site of cryolesion but the tracer soon clears from the animal. At 3 h postprobe injection, cell death probes PSS-794 and Annexin-Vivo 750 both produce high contrast signals at the site of cryoinjury. In the case of PSS-794, the image intensity at the site of cryoinjury is higher at the 3 h time point compared to the 0 h time point, indicating a relatively slow rate of probe accumulation on the surface of the dead and dying cells. As expected, the Annexin-Vivo 750 also showed extensive accumulation in the kidneys.[16,30] Target to nontarget (T/NT) quantification of in vivo images was performed by region of interest (ROI) analysis that compared the mean pixel intensities (MPI) at the cryoinjury site (T) to MPI at a nontarget site (NT) on the lower back (Figure 3). PSS-794 exhibited the highest T/NT at the 3 h time point (6.77 ± 0.47; T/NT ± SEM; $P < 0.003$) and then decreased. In contrast, the T/NT for Annexin-Vivo 750 increased incrementally to a value of 4.87 ± 0.54 at the 24 h end point, reflecting a slower rate of clearance from the nontarget site.

At 24 h after probe injection, the mice were sacrificed and subjected to ex vivo imaging and histological analysis. Ex vivo whole-body images were acquired with (1) the skin removed from the head, which exposed the tissue over the skull, and (2)


dx.doi.org/10.1021/cn3000197 | ACS Chem. Neurosci. 2012, 3, 530−537

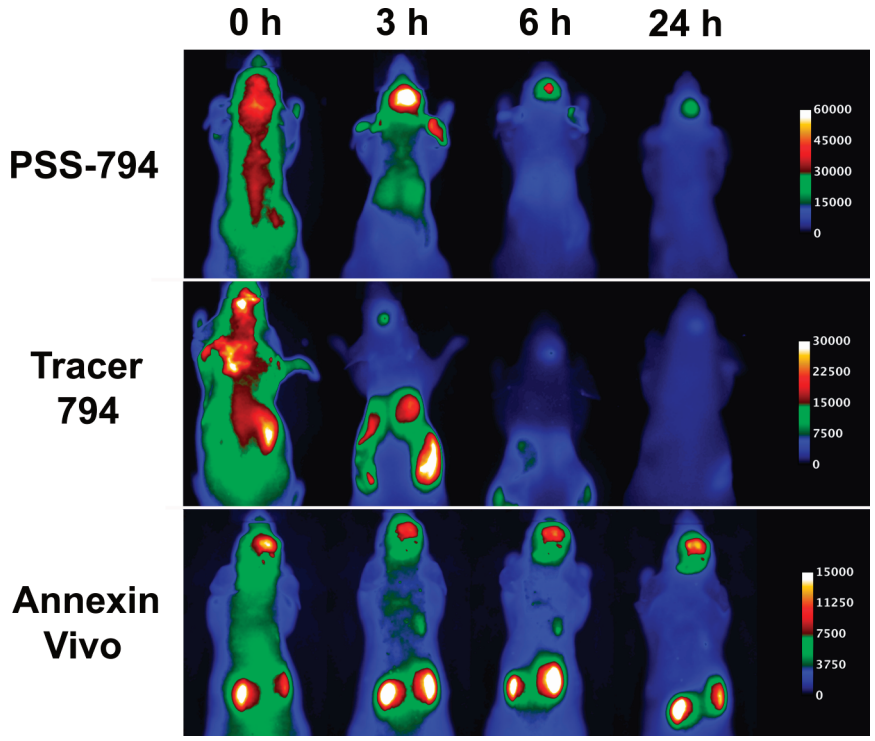


**Figure 2.** Representative in vivo near-infrared fluorescence montages of PSS-794, Tracer-794, and Annexin-Vivo 750 accumulation in a brain cryoinjury mouse model. A precooled metal cylinder was applied to the head of each mouse for 60 s followed by intravenous injection of either PSS-794 (3.0 mg/kg), Tracer-794 (3.0 mg/kg), or Annexin-Vivo 750. Images were acquired at the indicated time points after probe injection. $N = 5$.

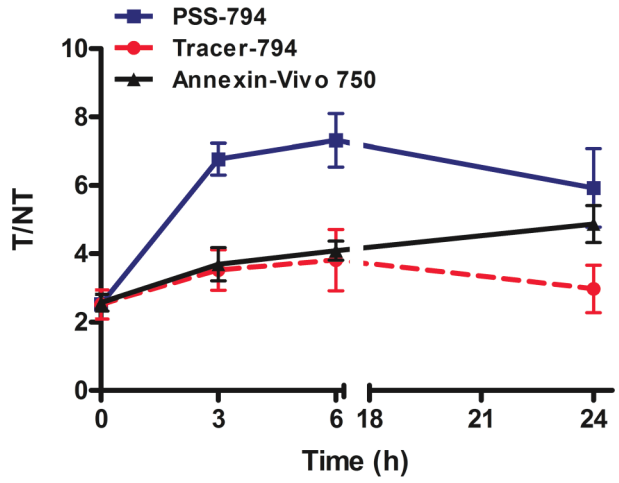


**Figure 3.** In vivo quantification of PSS-794, Tracer-794, and Annexin-Vivo 750 accumulating in a 60 s brain cryoinjury mouse model. Target to nontarget ratios (T/NT) were calculated by region of interest (ROI) analysis of the digital images. Shapes were drawn around the site of the cryoinjury (target, T) and around an equivalent site on the lower back (nontarget, NT) and the mean pixel intensities (MPI) were recorded. T/NT ± SEM $N = 5$. Numerical values and statistical significance are shown in Table S1 in the Supporting Information.

both the skin and the skull removed, which exposed the brain. ROI analysis compared the cryoinjury site in vivo just before animal sacrifice (labeled as Normal) to the deceased animal with skin removed (labeled as No Skin) and with both the skin and skull removed (labeled as No Skull). In each case, the MPI were recorded and normalized to the in vivo values. The normalized MPI for PSS-794 and Annexin-Vivo 750 decreased with each layer of tissue removed from the head (Figure S2, Table S2 in the Supporting Information). This is unusual because MPI at a deep-tissue site typically increases as the intervening skin and tissue is removed.[31] It appears that PSS-794 and Annexin-Vivo 750 target the cryolesion-induced cell death that is occurring on the skin, the pericranium, and on the brain. The normalized MPI for Tracer-794 images exhibited a different trend and increased with removal of the skin followed by a decrease in MPI with removal of the skull (Figure S2, Table S2 in the Supporting Information). But the absolute MPI for the Tracer-794 images were substantially lower than the values for the PSS-794 images ($P < 0.0005$ for Normal; $P < 0.001$ for No Skin; $P < 0.03$ for No Skull), reflecting the much greater clearance of tracer dye from the cryoinjury (Figure S3 in the Supporting Information). These spatial and temporal differences in probe localization indicate that the targeted cell death probe PSS-794 and nontargeted Tracer-794 accumulate in the brain cryoinjury by different mechanisms.

H&E micrographs of sectioned cryoinjured brains from mice sacrificed at 24 h after probe injection showed a focal region of cell death that was surrounded by healthy brain tissue (Figure 4A). Sections of cryoinjured brains were imaged using a fluorescence scanner to determine probe distribution throughout the brain. There was high accumulation of PSS-794 at the cryolesion site, while only negligible amounts of Tracer-794 were in the cryoinjured brain (Figure S4 in the Supporting Information). To further confirm that PSS-794 was targeting sites of brain cell death, immunohistochemisty was performed on the cryoinjured brains using an antibody specific for activated caspase-3. Fluorescence microscopy showed extensive staining of activated caspase-3 around the cryolesion, and also strong near-infrared fluorescence signal from the PSS-794 (Figure 4B). Caspase-3 and PSS-794 staining could not be visualized in healthy regions of the brain (Figure S6 in the


dx.doi.org/10.1021/cn3000197 | ACS Chem. Neurosci. 2012, 3, 530–537

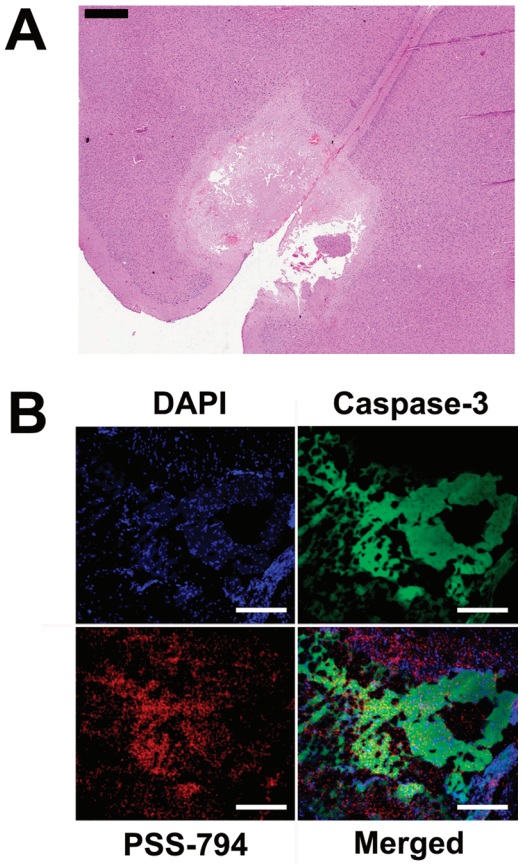


**Figure 4.** Representative histological micrographs from cryoinjured mouse brains. The micrographs were subjected either to H&E staining (A) or counterstained with an anticaspase-3 antibody and DAPI (B). Images in (B) are from the region of the brain cryoinjury. Scale bar in (A) = 500 $\mu$M. Scale bar in (B) = 200 $\mu$M.

Supporting Information). Fluorescence from Tracer-794 could not be detected in the same regions as caspase-3 in the cryoinjured brains (Figure S5 in the Supporting Information).

To determine if PSS-794 could measure TBI severity in vivo, the cryolesion experiment was repeated, with the time for contacting the precooled metal cylinder to the mouse's head reduced to 20 s. The animals were subsequently dosed with either PSS-794 or Tracer-794 and then imaged over time (Figure S7 in the Supporting Information). As shown in Figure 5 and Table S3 (Supporting Information), T/NT values for PSS-794 and Tracer-794 were lower in the 20 s cryolesion mouse model indicating less tissue damage compared to the 60 s cryolesion. Quantification of the ex vivo images with skin or skull removed showed similar PSS-794 and Tracer-794 staining patterns as with the 60 s cryolesion (Figures S2 and S8 in the Supporting Information).

Evans Blue is routinely used to monitor BBB disruption in animal models;[32,33] thus, it served as a positive control for Tracer-653 in this mouse TBI model. Separate cohorts of cryoinjured mice were administered Evans Blue and Tracer-653. Evans Blue extravasation is typically quantified using histology; however, we utilized its weak red fluorescence emission to perform ex vivo imaging of the brain sections.[34] The ex vivo images of cryoinjured brains clearly showed accumulation of Evans Blue at Day 0 and less so at Day 3 postinjury (Figure S12 in the Supporting Information). When compared to Tracer-653, the area of Evans Blue staining was

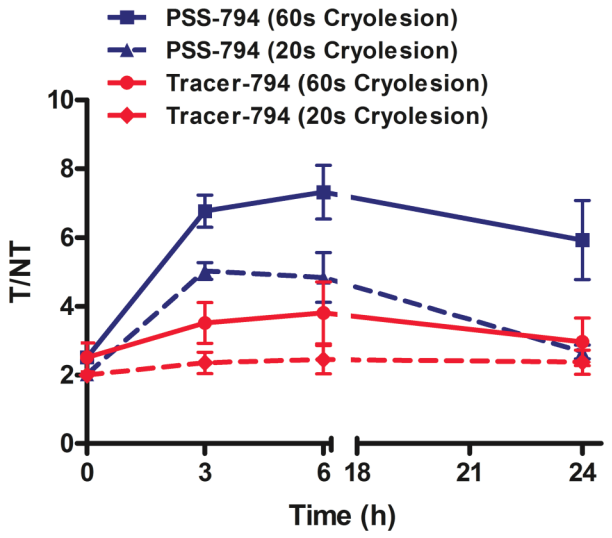


**Figure 5.** Comparison of PSS-794 and Tracer-794 accumulation in the 20 and 60 s brain cryoinjury mouse models. T/NT ratios were calculated by ROI analysis. T/NT ± SEM, $N$ = 5. Numerical values and statistical significance are shown in Table S3 in the Supporting Information.

more localized at the site of cryoinjury. In vivo, Evans Blue binds to albumin proteins, causing it to have a significantly higher molecular weight compared to Tracer-653 (67 vs 2 kDa).[35] The smaller effective size of Tracer-653 likely allows it to permeate into areas that are not accessible by the Evans-Blue–albumin complex, thus increasing the area of tissue that is stained by Tracer-653.[36,37] Taken together, the results indicate that Tracer-653 is an effective substitute for Evans Blue as a tracer probe for monitoring BBB disruption in TBI. Compared to Evans Blue, Tracer-653 exhibits a much brighter and more narrow, deep-red emission band and thus is more amenable to multicolor optical imaging.

To determine if we could simultaneously follow cranial cell death and BBB disruption in a single animal, we injected near-infrared PSS-794 and deep-red, Tracer-653 into mice that had received cryolesions. In short, three cohorts of hairless mice were administered 60 s brain cryolesions, and then injected with PSS-794 either immediately following cryoinjury, at 3 days postcryoinjury, or at 7 days postcryoinjury. Each mouse was also injected with Tracer-653 at 5 h post-PSS-794 injection (the injection lag time accounts for the difference in probe clearance rates). At 1 h after Tracer-653 injection, the mice were anesthetized and sacrificed. The brains were excised and placed in an epifluorescence imaging station for ex vivo imaging. As shown in Figure 6, the amount of PSS-794 accumulation in these cryoinjured brain sections decreased greatly with the age of the injury. For example, the MPI for a cryolesion section on Day 3 was 6-fold lower ($P$ < 0.0002) than the equivalent section on Day 0 (Figure S10 in the Supporting Information), indicating a substantial and relatively rapid decrease in the number dead and dying cells. In comparison the Tracer-653 signal in a cryoinjured brain decreased much more slowly with the age of injury. For example, the MPI for a cryolesion section on Day 7 was only about 2-fold lower ($P$ < 0.05) than the equivalent section on Day 0 (Figure 6 and Figure S10 in the Supporting Information). Furthermore, the amount of Tracer-653 in a cryoinjured brain on Day 7 (as judged by comparing MPI) was three times higher ($P$ < 0.05) than an equivalent brain taken from a healthy control mouse treated with Tracer-


dx.doi.org/10.1021/cn3000197 | ACS Chem. Neurosci. 2012, 3, 530–537

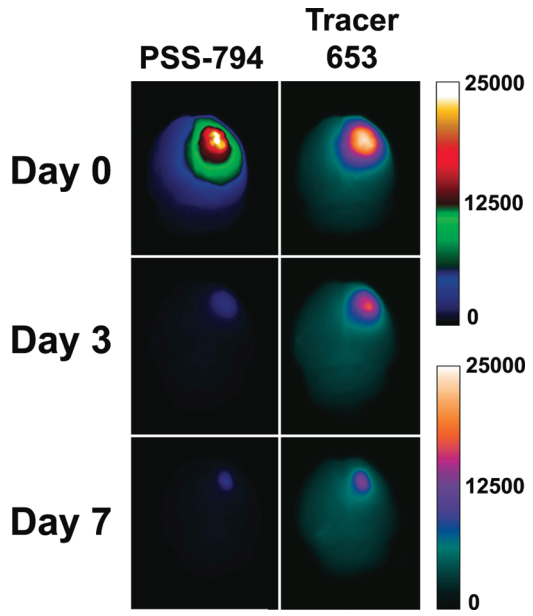


**Figure 6.** Multicolor fluorescence imaging of cell death and blood-brain-barrier disruption in cryoinjured brains. Three cohorts of hairless mice were given a 60 s brain cryoinjury. Mice were then injected with a single dose of PSS-794 either immediately following cryoinjury (Day 0), 3 days postcryoinjury (Day 3), or 7 days postcryoinjury (Day 7). Each mouse was also injected with Tracer-653 at 5 h post-PSS-794 injection. One hour after Tracer-653 injection, the mice were anesthetized and sacrificed. The brains were excised and placed in an epifluorescence imaging station for ex vivo imaging.

653 (Figure S11 in the Supporting Information). Taken together, the Tracer-653 data consistently indicates that there is a gradual but incomplete improvement in BBB integrity over the seven day postcryolesion period.

## DISCUSSION

The cryoinjury TBI mouse model used in these studies is a technically simple, high-throughput version of a previously reported model that contacts a precooled rod with the surgically exposed skull of mice.[38−40] We chose to not remove the skin around the skull because preliminary studies indicated that the cell death probes target the dead skin cells generated during the surgery, thus complicating the in vivo imaging. We find that the lesions caused by this adapted cryoinjury model are highly reproducible in size and location (Figure S3 in the Supporting Information) and can be clearly delineated from the rest of the brain.[41] However, this model only conditionally mimics human TBI and lacks the diffusion axonal injuries that complicate human head injuries.[42] Other TBI mouse models such as the controlled cortical impact and fluid percussion injury models can mimic the whole spectrum of focal-type brain injuries and produce axonal injuries.[43] But these models have technical drawbacks including the need for specialized equipment and the requirement to perform animal craniotomy.

We evaluated two tracers, Tracer-794 and Tracer-653, and two targeted probes, PSS-794 (2 kDa) and Annexin Vivo-750 (36 kDa), in the adapted cryolesion TBI model. The two targeted probes are functionally similar in that they identify dead and dying cells with membranes that expose phosphatidylserine; however, the probes are quite different in molecular size and blood clearance pathways. Annexin probes are known to accumulate in the kidneys, whereas PSS-794 clears more though the liver. The in vivo epifluorescence imaging showed that the maximum T/NT ratio with PSS-794 (6.77 ± 0.47) occurred at about 3 h after probe injection and was about 2 times higher than the maximum T/NT ratio with Annexin Vivo-750 (Figures 2 and 3). Both cell death probes cleared fairly slowly from the site of cryolesion. In comparison, Tracer-794 diffused in and completely out of the cryoinjury within a few hours. PSS-794 accumulation at the cryoinjury was observed to increase with injury severity, as judged by comparing the 20 and 60 s cryolesions (Figure 5). Thus, for preclinical studies that measure TBI severity in mouse models, optical imaging using PSS-794 appears to be a complementary alternate to classical methods that monitor changes in lesion volume.[44,45]

Multicolor fluorescence imaging is a promising new method to simultaneously monitor different physiological processes,[46,47] but has previously not been exploited to monitor TBI progression in mice. The highly fluorescent Tracer-653 functions like Evans Blue dye and allows optical imaging of BBB disruption. Furthermore, the deep-red emission of Tracer-653 can be distinguished from the near-infrared emission of PSS-794 in the same animal. Multicolor imaging of cryoinjured mice that were dosed with both PSS-794 and Tracer-653 enabled longitudinal tracking of the changes in cell death and BBB permeability, respectively. The PSS-794 images in Figure 6 and Figure S10 in the Supporting Information show that the amount of cell death had decreased substantially after Day 3, presumably due to efficient dead cell clearance by the animal's innate immune system.[48] But the Tracer-653 images indicate that healing and repair of the BBB was a much slower process. After Day 7, the BBB was still substantially more permeable than before the cryoinjury event, a time frame that is consistent with previous literature observations.[36,37]

In summary, we report that the synthetic near-infrared fluorescent probe, PSS-794, can be used to visualize cell death in an adapted cryolesion mouse model of TBI. The optical images with PSS-794 produced higher cryolesion signal contrast (higher T/NT ratio) than the mechanistically similar protein probe, Annexin-Vivo 750. Tracer-653 was validated as a low molecular weight, deep-red tracer dye for monitoring BBB disruption, and a binary mixture of PSS-794 and Tracer-653 was employed for multicolor imaging of cell death and BBB permeability in a single animal. The imaging data indicates that at 3 days after brain cryoinjury the amount of cell death had decreased significantly, but the integrity of the BBB was still impaired; at 7 days, the BBB was still substantially more permeable than before cryoinjury. The pathophysiological outcomes of TBI are highly heterogeneous in terms of severity and rate of progression. The time between physical trauma and the onset of secondary processes such as BBB breakdown is a potential window for therapeutic treatment.[49] It should be possible to develop this adapted cryoinjury mouse model into a high throughput, optical imaging screen of experimental therapeutics for TBI.

## METHODS

**Ethics Statement.** All animal experiments were approved for animal health, ethics, and research by the Animal Welfare Committee of Leiden University Medical Center and the Institutional Animal Care and Use Committee of the University of Notre Dame. All animals received humane care and maintenance in compliance with the *Code of Practice Use of Laboratory Animals in Cancer Research*.[50]

**Probe Synthesis.** The synthesis and properties of Tracer-794 ($\lambda_{ex}$, 794 nm; $\lambda_{em}$, 810 nm), PSS-794 ($\lambda_{ex}$, 794 nm; $\lambda_{em}$, 810 nm) , and Tracer-653 ($\lambda_{ex}$, 653 nm; $\lambda_{em}$, 673 nm) have been reported previously.[51,52] PSS-794 is commercially available as PSVue 794 (Molecular Targeting Technologies Inc., West Chester, PA). Annexin-Vivo 750 ($\lambda_{ex}$, 755 nm; $\lambda_{em}$, 772 nm) was purchased from PerkinElmer (Waltham, MA).

**Traumatic Brain Injury Mouse Models.** Two cohorts of 4−6 week old athymic mice (male, ∼25 g, *nu/nu*) ($n$ = 5) were anesthetized by 2−3% isoflurane inhalation. A metal cylinder, with a 3 mm diameter, was precooled in liquid nitrogen and applied to the parietal region of each mouse's head for either 20 or 60 s. The mice then received an intracardiac injection of either PSS-794 (3.0 mg/kg, 100 $\mu$L in 1% DMSO/$H_2O$) or Tracer-794 (3.0 mg/kg, 100 $\mu$L in $H_2O$). A cohort of athymic mice ($n$ = 5) was subjected to a 60 s cryoinjury and received an intracardiac injection of Annexin-Vivo 750.

To investigate the progression of blood-brain-barrier disruption and cell death in traumatic brain injury, three cohorts of immunocompetent hairless mice (male, 25 g, *SKH1-E*) (n = 4−5) were anesthetized by 2−3% isoflurane inhalation. A metal cylinder, with a 3 mm diameter, was precooled in liquid nitrogen and applied to the parietal region of each mouse's head for 60 s. The mice then received a retro-orbital injection of PSS-794 (3.0 mg/kg, 100 $\mu$L in 1% DMSO/$H_2O$) and placed back into their cages. Five hours later, the mice received a retro-orbital injection of Tracer-653 (2.0 mg/kg, 100 $\mu$L in $H_2O$). One hour later, the mice were anesthetized by isoflurane inhalation and placed inside an IVIS Lumina instrument (Caliper Life Sciences, Hopkinton, MA) configured for whole-body, epi-fluorescence imaging. After in vivo imaging, one cohort was sacrificed and ex vivo fluorescence imaging was performed on the excised brain. The other cohorts were placed back into their cages. Cohorts were subjected to the same PSS-794 and Tracer-653 injection and imaging procedures, either three or seven days postinjury (Figure S9 in the Supporting Information).

Evans Blue (Sigma, St. Louis, MO) (25 mg/kg, 100 $\mu$L in $H_2O$) was injected intravenously into hairless mice following 60 s brain cryolesion. The probe was allowed to circulate for 1 h, then the mice were anesthetized and sacrificed. The brains were excised and placed inside an IVIS Lumina instrument for ex vivo epi-fluorescence imaging. Another cohort of hairless mice were subjected to the same injection and imaging procedure 3 days postinjury.

**In Vivo Near-Infrared Fluorescence Imaging.** Athymic mice were anesthetized by 2−3% isoflurane inhalation and placed inside an IVIS Spectrum instrument (Caliper Life Sciences, Hopkinton, MA) configured for whole-body epifluorescence imaging. For mice injected with PSS-794 or Tracer-794, images were acquired immediately after probe injection and at 3, 6, and 24 h time points (excitation filter, 710 nm; emission filter, 820 nm; exposure time, 1 s; bin, 8; f/stop, 2; field of view, 6.6 cm). For mice injected with Annexin-Vivo 750, images were acquired for 1 s using a 710 nm excitation filter and a 780 nm emission filter (bin, 4; f/stop, 2; field of view, 6.6 cm). After each time point, the mice were returned to their cages and fed ad libitum.

Acquired images were exported as 16 bit tiff files and region of interest (ROI) analysis was performed using *ImageJ 1.44*. In short, a ROI was drawn around the cryoinjury site (T) and an equal sized ROI was drawn on the lower back (NT) of each mouse (Figure S1 in the Supporting Information). The mean pixel intensity of the T and NT was measured and recorded for each mouse. The T/NT ratios were then calculated, and statistical analysis was performed to acquire the average of each ratio (n = 5) with the standard error of the mean (SEM). The resulting ROI values were plotted using *Graphpad Prism 4*.

**Ex Vivo Near-Infrared Fluorescence Imaging.** Following the 24 h time point, mice were sacrificed by cervical dislocation. Ex vivo images were acquired with the skin from the head removed and both the skin and the skull removed to facilitate epifluorescence imaging with an IVIS Spectrum instrument (excitation filter, 710 nm; emission filter, 820 nm; exposure time, 1 s; bin, 8; f/stop, 2; field of view, 6.6 cm for PSS-794 and Tracer-794) (excitation filter, 710 nm; emission filter, 780 nm; exposure time, 1 s; bin, 4; f/stop, 2; field of view, 6.6 cm for Annexin-Vivo 750).

Immunocompetent hairless mice were sacrificed, and the brains excised and placed inside an IVIS Lumina instrument for multicolor epifluorescence imaging (excitation filter, 705−780 nm; emission filter, 810−885 nm; exposure time, 5 s; bin, 2; f/stop, 2; field of view, 5 cm for PSS-794) (excitation filter, 615−665 nm; emission filter, 695−770 nm; exposure time, 8 s; bin, 2; f/stop, 2; field of view, 5 cm for Tracer-653).

ROI analysis was performed by drawing an ROI around the cryoinjury site and recording the mean pixel intensity. The resulting mean pixel intensities were plotted using *Graphpad Prism 4*.

**Histology.** Brains were flash frozen in OCT (Tissue Tek, Torrance, CA), fixed in 4% formaldehyde, and cut into 10 $\mu$M paraffin sections. Tissue sections were mounted onto slides and imaged using a LI-COR Odyssey (LI-COR Biosciences, Lincoln, NE) scanner equipped with a 785 nm diode laser. Slides were also subjected to hematoxylin and eosin (H&E) staining to determine the extent of cell death and cellular morphological changes in the cerebral cortex. Selected brain sections were incubated overnight with a rabbit anti-human polyclonal caspase-3 antibody (Abcam Inc.; 1:50). The sections were then incubated with goat anti-rabbit IgG conjugated to Alexa-Fluor 488 (Invitrogen; 1:500) for 15 min, and counterstained with DAPI. Fluorescence images of the sections were acquired using a Nikon TE-2000 U epifluorescence microscope equipped with the appropriate UV (ex., 340/80 nm; em., 435/85 nm), GFP (ex, 450/90 nm; em., 500/50 nm), and near-infrared filters (ex., 710/75 nm; em., 810/90 nm). Fluorescence images were captured using *Metamorph* software (Universal) and analyzed using *ImageJ 1.44*.

**Statistical Analysis.** Results are depicted as mean ± standard error of the mean (SEM). Statistical analysis was performed using a Student's $t$ test.

## ■ ASSOCIATED CONTENT

### Ⓢ Supporting Information

Additional imaging data and quantitative analysis. This material is available free of charge via the Internet at http://pubs.acs.org.

## ■ AUTHOR INFORMATION


### Corresponding Author

*E-mail: smith.115@nd.edu (B.D.S.); c.w.g.m.lowik@lumc.nl (C.W.G.M.L.).

### Author Contributions

‖B.A.S. and B.X. contributed equally to this work.


### Author Contributions

B.A.S. and B.X. performed the research and analyzed the data; I.Q. conducted imaging studies; V.B. conducted histology; S.X. and E.L.C. synthesized the probes; E.R.V., M.H., and E.L.K., helped design the experiments, B.A.S., B.X., C.W.G.M.L., and B.D.S. wrote the article.


### Funding

This study was supported by the Center for Translational Molecular Medicine, project MUSIS (Grant 03O-202); NIH Grants R01GM059078 (B.D.S.) and T32GM075762 (B.A.S.), Volkswagen Grant I83443, and the ENCITE project 201842.


### Notes

The authors declare no competing financial interest.

## ■ ACKNOWLEDGMENTS


We thank the Notre Dame Histology Core and the Notre Dame Integrated Imaging Facility for preparation of histological sections and access to whole animal imaging equipment.

## REFERENCES


(1) Faul, M., Xu, L., Wald, M. M., and Coronado, V. G. (2010) Traumatic Brain Injury in the United States: Emergency Department Visits, Hospitalizations, and Deaths, 2002−2006. *National Center for Injury Prevention and Control, Centers for Disease Control and Prevention*, 1−71.

(2) Thurman, D. J., Alverson, C., Dunn, K. A., Dunn, K. A., Guerrero, J., and Sniezek, J. E. (1999) Traumatic Brain Injury in the United States: a Public Health Perspective. *J. Head Trauma Rehabil. 14*, 602−615.

(3) Werner, C., and Engelhard, K. (2007) Pathophysiology of Traumatic Brain Injury. *Br. J. Anaesth. 99*, 4−9.

(4) Kim, J. J., and Gean, A. D. (2011) Imaging for the Diagnosis and Management of Traumatic Brain Injury. *Neurotherapuetics 8*, 39−53.

(5) Wilson, J. R. F., and Green, A. (2009) Acute Traumatic Brain Injury: a Review of Recent Advances in Imaging and Management. *Eur. J. Trauma Emerg. Surg. 35*, 176−185.

(6) Chapon, C., Franconi, F., Lacoeuille, F., Hindré, F., Saulnier, P., Benoit, J. P., Le Jeune, J. J., and Lemaire, L. (2009) Imaging E-Selectin Expression Following Traumatic Brain Injury in the Rat using a Targeted USPIO Contrast Agent. *Magn. Reson. Mater. Phys. 22*, 167−174.

(7) Reshef, A., Shirvan, A., Shohami, E., Grimberg, H., Levin, G., Cohen, A., Trembovler, V., and Ziv, I. (2008) Targeting Cell Death In Vivo in Experimental Traumatic Brain Injury by a Novel Molecular Probe. *J. Neurotrauma 25*, 569−580.

(8) Kosaka, N., Ogawa, M., Sato, N., Choyke, P. L., and Kobyashi, H. (2009) *In Vivo* Real-Time, Multicolor, Quantum Dot Lymphatic Imaging. *J. Invest. Dermatol. 129*, 2818−2822.

(9) Yamamoto, N., Tsuchiya, H., and Hoffman, R. M. (2011) Tumor Imaging with Multicolor Fluorescent Protein Expression. *Int. J. Clin. Oncol. 16*, 84−91.

(10) Mitsunaga, M., Kosaka, N., Kines, R. C., Roberts, J. N., Lowy, D. R., Schiller, J. T., Ishihara, Y., Hasegawa, A., Choyke, P. L., and Kobayashi, H. (2011) *In Vivo* Longitudinal Imaging of Experimental Human Papillomavirus Infection in Mice with a Multicolor Fluorescence Mini-Endoscopy System. *Cancer Prev. Res. 4*, 767−773.

(11) Blankenberg, F. G. (2008) In Vivo Detection of Apoptosis. *J. Nucl. Med. 49*, 81S−95S.

(12) Zhao, M. (2009) In Vivo Apoptosis Imaging Agents and Strategies. *Anti-Cancer Agents Med. Chem. 9*, 1018−1023.

(13) Niu, G., and Chen, X. (2010) Apoptosis Imaging: Beyond Annexin V. *J. Nucl. Med. 51*, 1659−1662.

(14) Ntziachristos, V., Schellenberger, E. A., Ripoll, J., Yessayan, D., Graves, E., Bogdanov, A., Jr., Josephson, L., and Weissleder, R. (2004) Visualization of Antitumor Treatment by Means of Fluorescence Molecular Tomography with an Annexin V-Cy5.5 Conjugate. *Proc. Natl. Acad. Sci. U.S.A. 101*, 12294−12299.

(15) Beekman, C. A., Buckle, T., van Leeuwen, A. C., Valdés Olmos, R. A., Verheij, M., Rottenberg, S., and van Leewen, F. W. (2011) Questioning the Value of (99m)Tc-HYNIC-Annexin V Based Response Monitoring after Docetaxel Treatment in a Mouse Model for Hereditary Breast Cancer. *Appl. Radiat. Isot. 69*, 656−662.

(16) Vanderheyden, J. L., Liu, G. Z., He, J., Patel, B., Tait, J. F., and Hnatowich, D. J. (2006) Evaluation of 99mTc-MAG3-Annexin V: Influence of the Chelate on In Vitro and In Vivo Properties in Mice. *Nucl. Med. Biol. 33*, 135−144.

(17) Lederle, W., Arns, S., Rix, A., Gremse, F., Doleschel, D., Schmaljohann, J., Mottaghy, F. M., Kiessling, F., and Palmowski, M. (2011) Failure of Annexin-Based Apoptosis Imaging in the Assessment of Antiangiogenic Therapy Effects. *EJNMMI Res. 1*, 26.

(18) Burtea, C., Laurent, S., Lancelot, E., Ballet, S., Murariu, O., Rousseaux, O., Port, M., Vander Elst, L., Corot, C., and Muller, R. N. (2009) Peptidic Targeting of Phosphatidylserine for the MRI Detection of Apoptosis in Atherosclerotic Plaques. *Mol. Pharmaceutics 6*, 1903−1919.

(19) Zheng, H., Wang, F., Wang, Q., and Gao, J. (2011) Cofactor-Free Detection of Phosphatidylserine with Cyclic Peptides Mimicking Lactadherin. *J. Am. Chem. Soc. 131*, 15280−15283.

(20) Xiong, C., Brewer, K., Song, S., Zhang, R., Lu, W., Wen, X., and Li, C. (2011) Peptide-Based Imaging Agents Targeting Phosphatidylserine for the Detection of Apoptosis. *J. Med. Chem. 54*, 1825−1835.

(21) Hanshaw, R. G., and Smith, B. D. (2005) New Reagents for Phosphatidylserine Recognition and Detection of Apoptosis. *Bioorg. Med. Chem. 13*, 5035−5042.

(22) Smith, B. A., Akers, W. J., Leevy, W. M., Lampkins, A. J., Xiao, S., Wolter, W., Suckow, M. A., Achilefu, S., and Smith, B. D. (2010) Optical Imaging of Mammary and Prostate Tumors in Living Animals using a Synthetic Near Infrared Zinc(II)-Dipicolylamine Probe for Anionic Cell Surfaces. *J. Am. Chem. Soc. 132*, 67−69.

(23) Smith, B. A., Gammon, S. T., Xiao, S., Wang, W., Chapman, S., McDermott, R., Suckow, M. A., Johnson, J. R., Piwnica-Worms, D., Gokel, G. W., Smith, B. D., and Leevy, W. M. (2011) In Vivo Optical Imaging of Acute Cell Death using a Near-Infrared Fluorescent Zinc-Dipicolylamine Probe. *Mol. Pharmaceutics 8*, 583−590.

(24) Smith, B. A., Xiao, S., Wolter, W., Wheeler, J., Suckow, M. A., and Smith, B. D. (2011) In Vivo Targeting of Cell Death using a Synthetic Fluorescent Molecular Probe. *Apoptosis 16*, 722−731.

(25) Bahamni, P., Schellenberger, E., Klohs, J., Steinbrink, J., Cordell, R., Zille, M., Müller, J., Harhausen, D., Hofstra, L., Reutelingsperger, C., Farr, T. D., Dirnagl, U., and Wunder, A. (2011) Visualization of Cell Death in Mice with Focal Cerebral Ischemia using Fluorescent Annexin A5, Propidium Iodide, and TUNEL Staining. *J. Cereb. Blood Flow Metab. 31*, 1311−1320.

(26) O'Neil, E. J., and Smith, B. D. (2004) Anion Recognition using Dimetallic Coordination Complexes. *Coord. Chem. Rev. 250*, 3068−3080.

(27) Abulrob, A., Brunette, E., Slin, J., Baumann, E., and Stanimirovic, D. (2008) Dynamic Analysis of the Blood-Brain Barrier Disruption in Experimental Stroke using Time Domain In Vivo Fluorescence Imaging. *Mol. Imaging 7*, 248−262.

(28) Hawkins, B. T., and Egleton, R. D. (2006) Fluorescence Imaging of Blood-Brain Barrier Disruption. *J. Neurosci. Methods 151*, 262−267.

(29) Murakami, K., Kondo, T., Yang, G., Chen, S. F., Morita-Fujimura, Y., and Chan, P. H. (1999) Cold Injury in Mice: a Model to Study Mechanisms of Brain Edema and Neuronal Apoptosis. *Prog. Neurobiol. 57*, 289−299.

(30) Lin, K. J., Wu, C. C., Pan, Y. H., Chen, F. H., Fu, S. Y., Chiang, C. S., Hong, J. H., and LoJ. M. (2012) In Vivo Imaging of Radiation-Induced Tissue Apoptosis by 99mTc(I)-his$_6$-Annexin A5. *Ann. Nucl. Med. 26*, DOI: 10.1007/s12149-012-0571-x

(31) Leblond, F., Davis, S. C., Valdés, P. A., and Pogue, B. W. (2010) Pre-Clinical Whole-Body Fluorescence Imaging: Review of Instruments, Methods and Applications. *J. Photochem. Phototbiol., B 98*, 77−94.

(32) Belayev, L., Busto, R., Zhao, W., and Ginsberg, M. D. (1996) Quantitative Evaluation of Blood-Brain Barrier Permeability Following Middle Cerebral Artery Occlusion in Rats. *Brain Res. 739*, 88−96.

(33) Del Valle, J., Camins, A., Pallás, M., Vilaplana, J., and Pelegri, C. (2008) A New Method for Determining Blood-Brain Barrier Integrity Based on Intracardiac Perfusion of an Evans Blue-Hoechst Cocktail. *J. Neurosci. Methods 174*, 42−49.

(34) Saria, A., and Lundberg, J. M. (1983) Evans Blue Fluorescence: Quantitative and Morphological Evaluation of Vascular Permeability in Animal Tissues. *J. Neurosci. Methods 8*, 41−49.

(35) Wolman, M., Klatzo, I., Chui, E., Wilmes, F., Nishimoto, K., Fujiwara, K., and Spatz, M. (1981) Evaluation of the Dye-Protein Tracers in Pathophysiology of the Blood-Brain Barrier. *Acta Neuropathol. 54*, 55−61.

(36) Habgood, M. D., Bye, N., Dziegielewska, K. M., Ek, C. J., Lane, M. A., Potter, A., Morganti-Kossmann, C., and Saunders, N. R. (2007) Changes in Blood-Brain Barrier Permeability to Large and Small Molecules Following Traumatic Brain Injury in Mice. *Eur. J. Neurosci. 25*, 231−238.

(37) Lotocki, G., Rivero Vaccari, J. P., Perez, E. R., Sanchez-Molano, J., Furones-Alonso, O., Bramlett, H. M., and Dietrich, W. D. (2009)

Alterations in Blood-Brain Barrier Permeability to Large and Small Molecules and Leukocyte Accumulation after Traumatic Brain Injury: Effects of Post-Traumatic Hypothermia. *J. Neurotrauma 26*, 1123−1134.
(38) Raslan, F., Schwarz, T., Meuth, S. G., Austinat, M., Bader, M., Renné, T., Roosen, K., Stoll, G., Sirén, A. L., and Kleinschnitz, C. (2010) Inhibition of Bradykinin Receptor B1 Protects Mice from Focal Brain Injury by Reducing Blood-Brain Barrier Leakage and Inflammation. *J. Cereb. Blood Flow Metab. 30*, 1477−1486.
(39) Stoffel, M., Blau, C., Reinl, H., Breidt, J., Gersonde, K., Baethmann, A., and Plesnila, N. (2004) Identification of Brain Tissue Necrosis by MRI: Validation by Histomorphometry. *J. Neurotrauma 21*, 733−740.
(40) Spaeth, N., Wyss, M. T., Weber, B., Scheidegger, S., Lutz, A., Verwey, J., Radovanovic, I., Pahnke, J., Wild, D., Westera, G., Weishaupt, D., Hermann, D. M., Kaser-Hotz, B., Aguzzi, A., and Buck, A. (2004) Uptake of 18F-Fluorocholine, 18F-Fluoroethyl-L-Tyrosine, and 18F-FDG in Acute Cerebral Radiation Injury in the Rat: Implications for Separation of Radiation Necrosis from Tumor Recurrence. *J. Nucl. Med. 45*, 1931−1938.
(41) Albert-Weissenberger, C., and Sirén, A. L. (2010) Experimental Traumatic Brain Injury. *Exp. Transl. Stroke Med. 2*, 16−23.
(42) Gaetz, M. (2004) The Neurophysiology of Brain Injury. *Clin. Neurophysiol. 115*, 4−18.
(43) O'Connor, W. T., Smyth, A., and Gilchrist, M. D. (2011) Animal Models of Traumatic Brain Injury: a Critical Evaluation. *Pharmacol. Ther. 130*, 106−113.
(44) Eriskat, J., Fürst, M., Stoffel, M., and Baethmann, A. (2003) Correlation of Lesion Volume and Brain Swelling from a Focal Brain Trauma. *Acta Neurochir. 86*, 265−266.
(45) Like any cell death probe, PSS-794 will target all accessible dead and dying tissues, which in this case is the skin and pericranium above the brain cryoinjury. The intervening signal is a potential drawback to the use of PSS-794 for planar, whole-body, fluorescence imaging. In principle, the problem can be circumvented by employing fluorescence tomography to quantify the separate amounts of PSS-794 at the different anatomical locations.
(46) Kobayashi, H., Hama, Y., Koyama, Y., Barrett, T., Regino, C. A., Urano, Y., and Choyke, P. L. (2007) Simultaneous Multicolor Imaging of Five Different Lymphatic Basins using Quantum Dots. *Nano Lett. 7*, 1711−1716.
(47) Yang, M., Jiang, P., and Hoffman, R. M. (2007) Whole-Body Subcellular Multicolor Imaging of Tumor-Host Interaction and Drug Response in Real Time. *Cancer Res. 67*, 5195−5200.
(48) Giulian, D., Chen, J., Ingeman, J. E., George, J. K., and Noponen, M. (1989) The Role of Mononuclear Phagocytes in Wound Healing After Traumatic Injury to Adult Mammalian Brain. *J. Neurosci. 9*, 4416−4429.
(49) Shloesberg, D., Benifa, M., Kaufer, D., and Friedman, A. (2010) Blood-Brain Barrier Breakdown as a Therapeutic Target in Traumatic Brain Injury. *Nat. Rev. Neurol. 6*, 393−403.
(50) Netherlands Inspectorate for Health Protection, Commodities and Veterinary Public Health (1999) Code of Practice Animal Experiments in Cancer Research. *Inspectie W&V*, 1−22.
(51) Leevy, W. M., Gammon, S. T., Jiang, H., Johnson, J. R., Maxwell, D. J., Jackson, E. N., Marquez, M., Piwnica-Worms, D., and Smith, B. D. (2006) Optical Imaging of Bacterial Infection in Living Mice using a Near-Infrared Molecular Probe. *J. Am. Chem. Soc. 128*, 16476−16477.
(52) Cole, E. L., Arunkumar, E., XiaoS., Smith, B. A., and Smith, B. D. (2011) Water-Soluble, Deep-Red Fluorescent Squaraine Rotaxanes. *Org. Biomol. Chem.* published online Nov 22, 2011. DOI: 10/1039/c2ob06783h.